frontiers in Physics

ORIGINAL RESEARCH
published: 13 May 2021
doi: 10.3389/fphy.2021.665956

Ligand-Free BaF_2: Nd Nanoparticles With Low Cytotoxicity, High Stability and Enhanced Fluorescence Intensity as NIR-II Imaging Probes

Xiaoxia Cui [1,2], Yantao Xu [1,2], Shengfei She [1,2], Xusheng Xiao [1,2], Chaoqi Hou [1,2] and Haitao Guo [1,2]**

[1] State Key Laboratory of Transient Optics and Photonics, Xi'an Institute of Optics and Precision Mechanics, Chinese Academy of Science (CAS), Xi'an, China, [2] Center of Materials Science and Optoelectronics Engineering, University of Chinese Academy of Sciences (UCAS), Beijing, China

Ligand-free BaF_2:Nd nanoparticles (NPs) with a size of 10 nm were fabricated by a novel synthetic route in the liquid phase. A transparent dispersion of the BaF_2:Nd NPs mixed with propanetriol and DMSO-d6 was done. Highly stable and outstanding near-infrared (NIR) fluorescence centered at 1,058 nm was detected using an excitation wavelength of 808 nm laser. Moreover, the dispersion can be found to be stable for over 1 month, and the cytotoxicity of the BaF_2:Nd NP dispersion has also been studied by 3-(4,5-dimethyl-2-thiazolyl)-2,5-diphenyl-2H-tetrazolium bromide (MTT) assay. The superior performance of these NPs exhibits their great potential application in high-contrast and high-penetration *in vivo* imaging.

Keywords: BaF_2:Nd, fluorescence imaging, stability, low toxicity, NIR-II

OPEN ACCESS

Edited by:
Peng Gao,
Xidian University, China

Reviewed by:
Xiaobao Yao,
The First Affiliated Hospital of Xi'an Jiaotong University, China
Zhiguang Zhou,
NewSpec Pty Ltd., Australia

****Correspondence:***
Xiaoxia Cui
cuixx@opt.ac.cn
Haitao Guo
guoht_001@opt.ac.cn

Specialty section:
This article was submitted to Optics and Photonics, a section of the journal Frontiers in Physics

Received: *09 February 2021*
Accepted: *14 April 2021*
Published: *13 May 2021*

Citation:
Cui XX, Xu YT, She SF, Xiao XS, Hou CQ and Guo HT (2021) Ligand-Free BaF_2: Nd Nanoparticles With Low Cytotoxicity, High Stability and Enhanced Fluorescence Intensity as NIR-II Imaging Probes. Front. Phys. 9:665956. doi: 10.3389/fphy.2021.665956

INTRODUCTION

Fluorescence imaging exhibits high sensitivity. Non-invasive and real-time monitoring has been regarded as one of the most promising optical imaging technologies in clinical applications [1]. However, at present, in general, the use of fluorescence imaging is limited due to the strong effect of scattering and absorption of the light by tissues. The image resolution is poor when the visible light-emitting fluorescence probes are employed, since the high scattering loss and autofluorescence observed from the biosamples will reduce the background ratio (SBR) of fluorescence images [2]. The light observed in the near-infrared (NIR) range of 700–950 and 1,000–1,700 nm is considered as the transparency window for bioimaging because the low scattering loss and reduced absorption coefficient are observed from the endogenous molecules [3, 4]. This light can exhibit infrared fluorescence of high brightness, deep tissue penetration, and clear images with high spatial resolution [5–7]. In the NIR imaging system, the fluorescence probe has become the most critical factor to achieve high-quality images. Therefore, the development of the novel NIR probe is becoming important particularly for future clinical applications.

Up to now, various NIR imaging probes (including quantum dots [8, 9], upconversion nanoparticles (NPs) [10–13], and rare earth-doped down-emission NPs [14, 15]) have been reported. However, the high biotoxicity and low quantum efficiency will limit further applications of NPs. Furthermore, for most upconversion NPs based on the $NaYF_4$ matrix, the light with an excitation wavelength of 980 nm causes overheating of tissues due to its matching wavelength with

the absorption of water [16, 17]. The NPs doped with rare earth ions, such as Nd^{3+}, Er^{3+}, and Ho^{3+}, have attracted greater attention because of their emission wavelength in the NIR-II region of 1,000–1,700 nm under the excitation wavelength of 800 nm. Imaing with these probes not only can avoid the heat accumulation in the tissues but also can reduce the biotoxic components and enhance the image quality due to the high penetration depth and spatiotemporal resolution [4, 18, 19].

The ideal fluorescence probe must satisfy the following criteria: First, it should achieve an enhanced emission intensity in the range of 1,000–1,700 nm, long life time, and high luminescence stability. Second, proper size should be fabricated to not only prevent the rapid renal excretion but also reduce the surface quenching effect. Third, it should exhibit high biocompatibility and low biotoxicity. In order to improve the biocompatibility of NPs, the NPs are usually modified by organic surfactants, which may reduce the luminescence intensity because of the quenching effect of the –CH and –OH groups [20]. In this article, BaF_2:Nd NPs were prepared without the use of organic ligand by the solvothermal method to improve the luminescence intensity at 1,058 nm. The BaF_2:Nd NP dispersions in dimethyl sulfoxide (DMSO)/propanetriol were produced with characteristics such as high stability and low biotoxicity. High biocompatibility and the penetration depth of imaging in the pork tissues have been evaluated. Furthermore, the NIR excitation ($\lambda_{ex} = 800$ nm), NIR emission ($\lambda_{em} = 1{,}058$ nm), and high photostability characteristics of the NPs are essential for performing deep tissue imaging in the near future.

EXPERIMENTAL

Material

Ba $(NO_3)_2{\cdot}6H_2O$ (99.9%, Alfa Aesar reagent), Nd $(NO_3)_3{\cdot}6H_2O$ (95%, Alfa Aesar reagent), NaF (99.99%, Alfa Aesar reagent), absolute ethanol (AR, Xian chemical regent Lo.), DMSO, and propanetriol (AR, Alfa Aesar reagent) were used without further purification. Ultrapure distilled and deionized water was used for the preparation of all solutions used in the following experiments.

Synthesis of BaF_2:Nd Nanoparticles

Ligand-free BaF_2:Nd NPs with a doping concentration of 3 mol% were prepared by a modified hydrothermal route [21]: 0.97 mmol of Ba $(NO_3)_2$ and 0.03 mmol of Nd $(NO_3)_3$ were first mixed with 40 mL of water. The solution was stirred thoroughly for 30 min at room temperature, and then 0.08 g of NaF was added to the aforementioned solution under stirring. Finally, 40 mL of ethanol was added and mixed; the mixed solution was again stirred for 10 min and then transferred to a Teflon-lined autoclave. Then, the autoclave was sealed and heated at 170°C for 10 h. The reactor was cooled to room temperature. The products were centrifuged and washed several times by ethanol and acetone. The residual precipitate was dried at 65°C under vacuum for 2 days.

Different concentrations of NP dispersions were prepared by adding 2–15 mg of BaF_2:Nd NPs powder to 0.2 mL of DMSO-d6 solvent. Then, the mixture was subjected to ultrasonication for 15 min, and finally 0.3 mL of propanetriol was added into the abovementioned mixture. The resulting transparent and stable dispersions were fabricated.

Characterization

X-ray diffraction (XRD) patterns of the samples were measured on a Bruker Advance powder X-ray diffractometer *via* a Cu Kα radiation. TEM analysis was performed using JEOL JEM-2100 field emission transmission electron microscope (TEM) at an acceleration voltage of 200 kV. Fourier Transform infrared (FTIR) spectra were determined on a Bruker FTIR spectrometer using transparent KBr wafers. All NPs were dried under vacuum prior to the formation of the KBr wafers and subsequent analysis. The absorption spectra were recorded in the range of 300–1,300 nm by the UV–Vis–NIR spectrophotometer (Shimadzu UV-3600) at room temperature. The fluorescence spectra were measured by a Zolix Omni-k 300 spectrophotometer using 800-nm laser diode pumps. Luminescence decay time of the sample was detected by a 300-MHz Tektronix oscilloscope (Model 3032B). Fluorescence images of NP powders and NP dispersions were captured by an NIR-II imaging system (GuangYingMei Co., Wuhan, China) equipped with InGaAs detector and 808-nm laser diode (the average power density is 80 mW/cm^2). The morphologies of the erythrocytes and platelets were characterized by optical microscope.

Hemolysis Assay

The BaF_2:Nd NP dispersions in phosphate buffer saline (PBS) were prepared with a concentration of 400 μgmL^{-1}. The red blood cells (RBCs) were collected by centrifuging the anticoagulated human whole blood samples at 1,000 rpm for 5 min. Then, RBC suspensions in PBS with a concentration of 2% were prepared. About 2.5 mL of NP dispersions was incubated with 2.5 mL of RBC suspensions (2%) for 2 h at 37°C. The control groups with positive and negative samples were prepared by mixing 2.5 mL of RBC suspensions with 2.5 mL of distilled water and saline water, respectively. After incubation, the samples were centrifuged, and the absorbance of the supernatant was measured at 570 nm. The percentage rate of hemolysis was calculated as follows: Hemolysis rate % $= (OD_{test} - OD_{neg})/(OD_{pos} - OD_{neg})$, where OD_{test}, OD_{neg}, and OD_{pos} are the absorbance of the test sample, absorbance of the negative control (saline), and absorbance of the positive control (water), respectively. All data were obtained based on the average of five replications.

Erythrocyte Morphology

The RBCs were collected by centrifuging fresh anticoagulant human blood and washing it three times with PBS. Then, 20 μL of RBC suspensions was incubated with 1 mL of BaF_2:NP dispersions (100 $\mu g{\cdot}mL^{-1}$) at room temperature for 30 min. Finally, the RBCs were again washed three times with PBS. The morphologies of RBCs were observed under the optical microscope.

MTT Assay

3-(4,5-dimethyl-2-thiazolyl)-2,5-diphenyl-2H-tetrazolium bromide (MTT) assay was performed to measure cell viability after MTT interaction with NPs under different conditions [22].

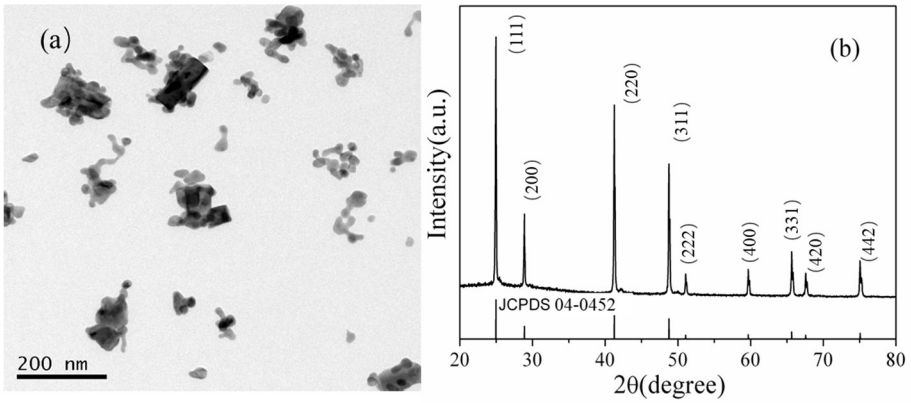

FIGURE 1 | TEM images **(a)** and XRD patterns **(b)** of BaF_2:Nd (3 mol%) NPs.

The HeLa cells were placed in 96-well plates and incubated under the atmosphere of 5% CO_2 at 37°C until the monolayer of cell was formed at the bottom of the well (96-well flat plate). After 2 h, different concentrations (50, 100, 150, and 200 μgmL^{-1}) of NP dispersions in PBS were added when the cell adhered to the well. The mixture was incubated in 5% CO_2 at 37°C for 48 h, and 20 μL of the MTT solution (5 mg/mL) was added to each well and cultured for 4 h. After completion of the culture, the medium was carefully discarded and the precipitates were retained. Then, 0.5 mL of DMSO was added to each well and centrifuged at low speed for 10 min to make the crystal dissolve completely. Finally, the solution was transferred into separate wells in a 96-well-plate, and the absorbance values were measured at 540 nm in a spectrophotometer. At the same time, back sample (containing culture medium, MTT, DMSO) and control sample (containing cells, PBS, culture medium, MTT, DMSO) were prepared. The percentage viability of HeLa cells incubated with NPs was calculated as $[A]_{test}/[A]_{control} \times 100$, where $[A]_{test}$ is the absorbance of the tested sample incubated with NPs and $[A]_{control}$ is the absorbance of the control sample.

Imaging in the Phantom and Pork Tissue

The fluorescence imaging was performed by a NIR *in vivo* imaging system equipped with an InGaAs detector. The excitation wavelength of LD laser was 808 nm and the excitation intensity was 80 $mW{\cdot}cm^{-2}$. In order to avoid the interference of excitation lights, 850 nm long-pass filter and 1,060 nm band-pass filter were employed, thus enhancing the image intensity at 1,060 nm. The temperature of detector chip was adjusted as −35°C. Before the imaging technique, the BaF_2:Nd NP dispersion was filled to a capillary based on the capillary phenomenon immersed in the dispersions. Then, the capillary was sealed with black glass cement and was inserted into the hole of the phantom and the pork tissues. The fluorescence signals of BaF_2:Nd NPs present in the phantom and the pork tissues were captured under the excitation wavelength of 808 nm.

Ethics

The studies involving human participants were reviewed and approved by the Ethics Committee of First Affiliated Hospital of Xi'an Jiaotong University. The A written informed consent was obtained from the patients/participants involved in this study.

RESULTS AND DISCUSSION

Nanoparticle Characterization

Figure 1a shows the TEM images of the obtained NPs. The NPs exhibit an average size of about 16 ± 1 nm and high dispersity. The crystal structural characteristics of the samples were evaluated by the XRD patterns. The diffraction patterns perfectly matched with that of the standard JCPDS Card (No. 04-0452) of the BaF_2 crystal, as shown in **Figure 1b**. There were no other impurity peaks found in the diffraction patterns, and the powders were crystallized in a pure face-centered cubic phase.

Figure 2 shows the FTIR spectrum of BaF_2:Nd nanopowders. It can be seen that BaF_2:Nd NPs show obvious absorption peaks at 3,460, 2,025, 1,675, and 1,207 cm^{-1}. The broad absorption peaks at 3,460 and 1,675 cm^{-1} correspond to the vibration absorption of –OH ions in the water molecules. The absorption bands centered at 1,138 and 1,207 cm^{-1} are attributable to the stretching vibration of the C–O bond. The absorption band centered at 2,025 cm^{-1} is due to the stretching vibration of the C–C bond. Based on the abovementioned results, it can be concluded that the surface of the BaF_2:Nd NPs prepared by the hydrothermal method is covered with –OH groups and C–O groups, which greatly improve the hydrophilicity in DMSO-d6/propanetriol solvent.

Figure 3a shows the absorption spectrum of the BaF_2:Nd nanocrystal dispersion. All five absorption bands correspond to the Nd^{3+} transitions from $^4I_{9/2}$ ground state to various excited states of the $^4F_3$ electronic configuration. The emission spectrum of the BaF_2:Nd NPs was measured at the excitation wavelength of 808 nm (**Figure 3b**). All the observed emission peaks are the principal transitions from the $^4F_{3/2}$ level to the $^4I_{9/2}$, $^4I_{11/2}$, and $^4I_{13/2}$ levels [23]. The bands centered at 894 nm are assigned

to the transitions of $^4F_{3/2} \rightarrow {}^4I_{9/2}$, while the bands centered at 1,056 nm are due to the transitions of $^4F_{3/2} \rightarrow {}^4I_{11/2}$ levels.

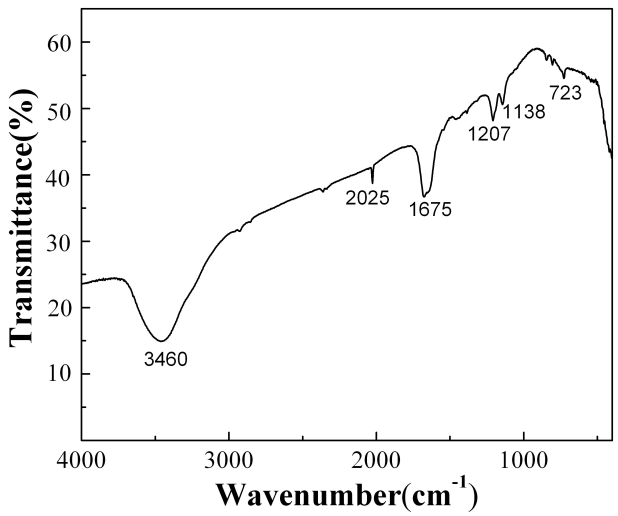

FIGURE 2 | FTIR spectrum of BaF_2:Nd (3 mol%) nanopowders.

Figure 3c shows the decay curve of Nd^{3+} ion for the $^4F_{3/2} \rightarrow {}^4I_{11/2}$ transition in the BaF_2:Nd NP dispersions. A long lifetime was calculated as 135 μs by fitting the decay curve with second exponential function. The long lifetime helps to reduce the imaging noise induced by autofluorescence. **Figure 3d** shows the NIR fluorescence image of the BaF_2:Nd nanocrystal dispersion. The uniform distribution of NP dispersions in terms of optical intensity exhibits their excellent optical and physical stabilities.

To detect the physical stability of the BaF_2:Nd NP probes for NIR-II imaging *in vivo*, the transmittance of the NP dispersion with high mass concentration (30 mg/mL) was monitored for 30 days (**Figure 4**). Obviously, the NPs can form a transparent dispersion in DMSO and propanetriol, which remain uniform and steady for 30 days without any special treatment. These results are consistent with the results of NIR images, as shown in **Figure 3d**.

Biocompatibility Study

Hemolysis Assay

The biotoxicity of the NPs can be characterized by determining the extent of hemolysis. Based on the experimental results of the absorption spectra shown in **Figures 5A–C**, the Hemolysis

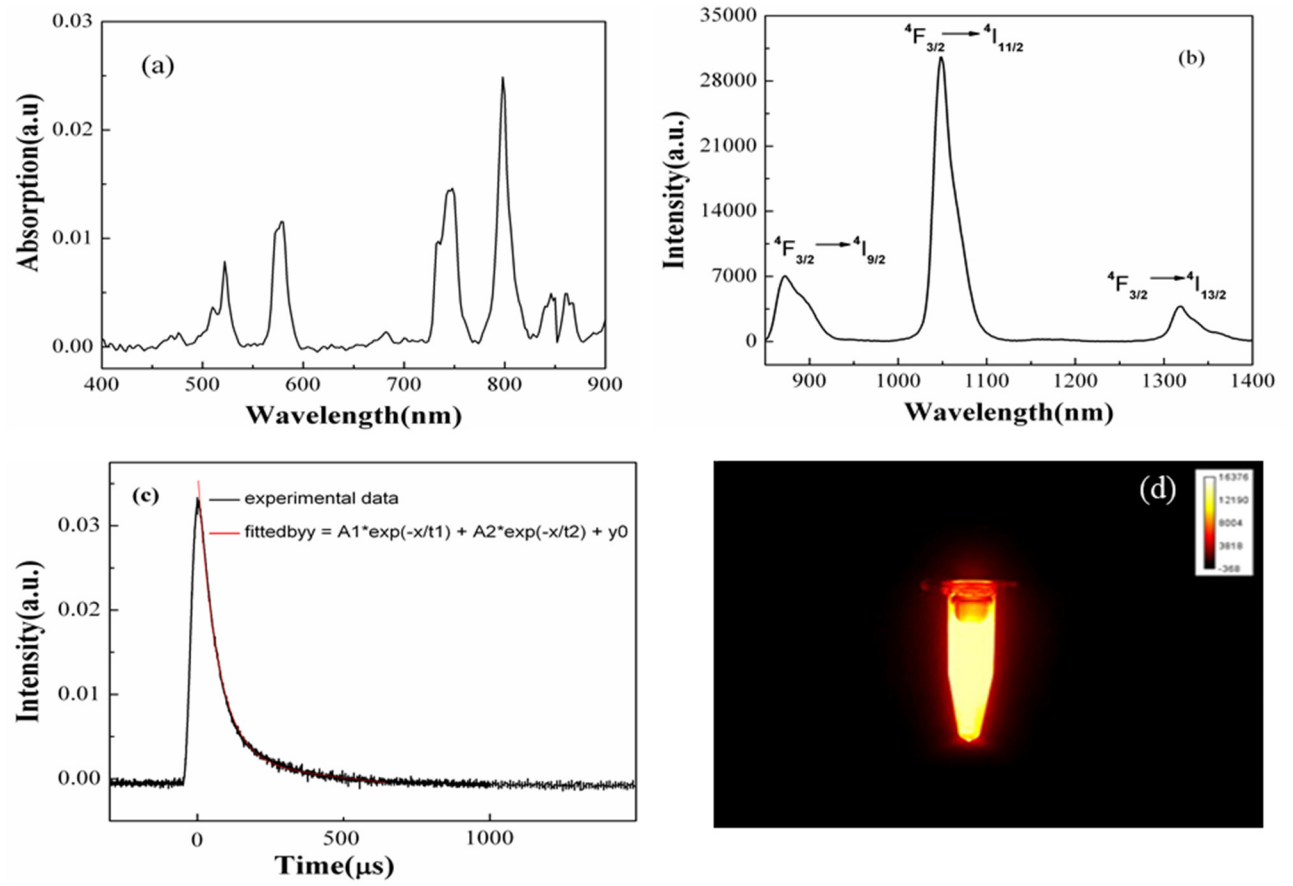

FIGURE 3 | Absorption spectrum **(a)**, emission spectrum **(b)**, decay curve **(c)**, and NIR image **(d)** of the BaF_2:Nd NP dispersion in DMSO-d6/propanetriol solvents (10 mg/mL).

rate (HR) values of the tested specimens were calculated as 3.27%, which is less than the safe value of 5% (ISO10993-4 standard). Such results prove that the BaF_2:Nd NPs are non-hemolytic and that they can be used in future clinical imaging diagnosis.

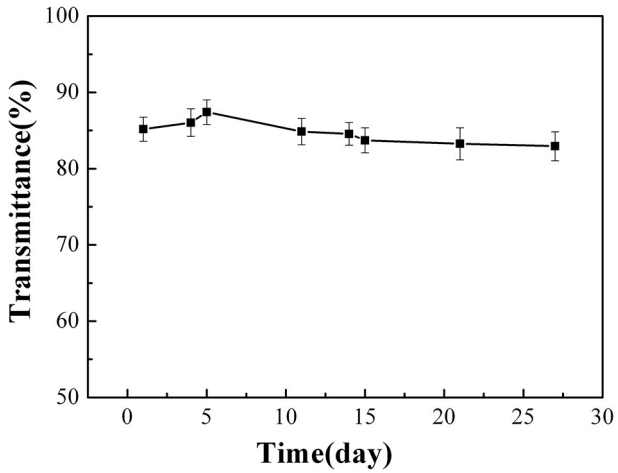

FIGURE 4 | The transmittance of BaF_2:Nd NP dispersions (30 mg/mL) depends on different times.

MTT Assay

The cytotoxicity of the BaF_2:Nd NP dispersions has been evaluated by MTT assay using HeLa cells. Obviously, no cytotoxicity of NP dispersions at a high concentration of 200 μg/mL is observed. As shown in **Figure 5D**, the survival rate of HeLa cells is 91% after incubation with BaF_2:Nd NP dispersions (200 μg/mL) for 48 h. In the case of 50 μg/mL, the survival rate was improved to 97%. These data show satisfactory results on the biocompatibility of the BaF_2:Nd NPs for *in vitro* imaging.

The morphological changes in RBCs are usually used as a marker to analyze the pathological condition of diseases. The normal RBCs are elliptical and sunken on both sides in saline water. When the cells interact with toxic exogenous substances, the morphological changes, such as swelling, spike growth, and even death, in RBCs occur. **Figure 6** shows the morphologies of RBCs before and after incubation with BaF_2:Nd NPs. It can be seen that the RBCs in the experiment do not show additional morphological change (**Figure 6b**) compared with those in the control group (**Figure 6a**). It implies that the BaF_2:Nd NPs possess low toxicity.

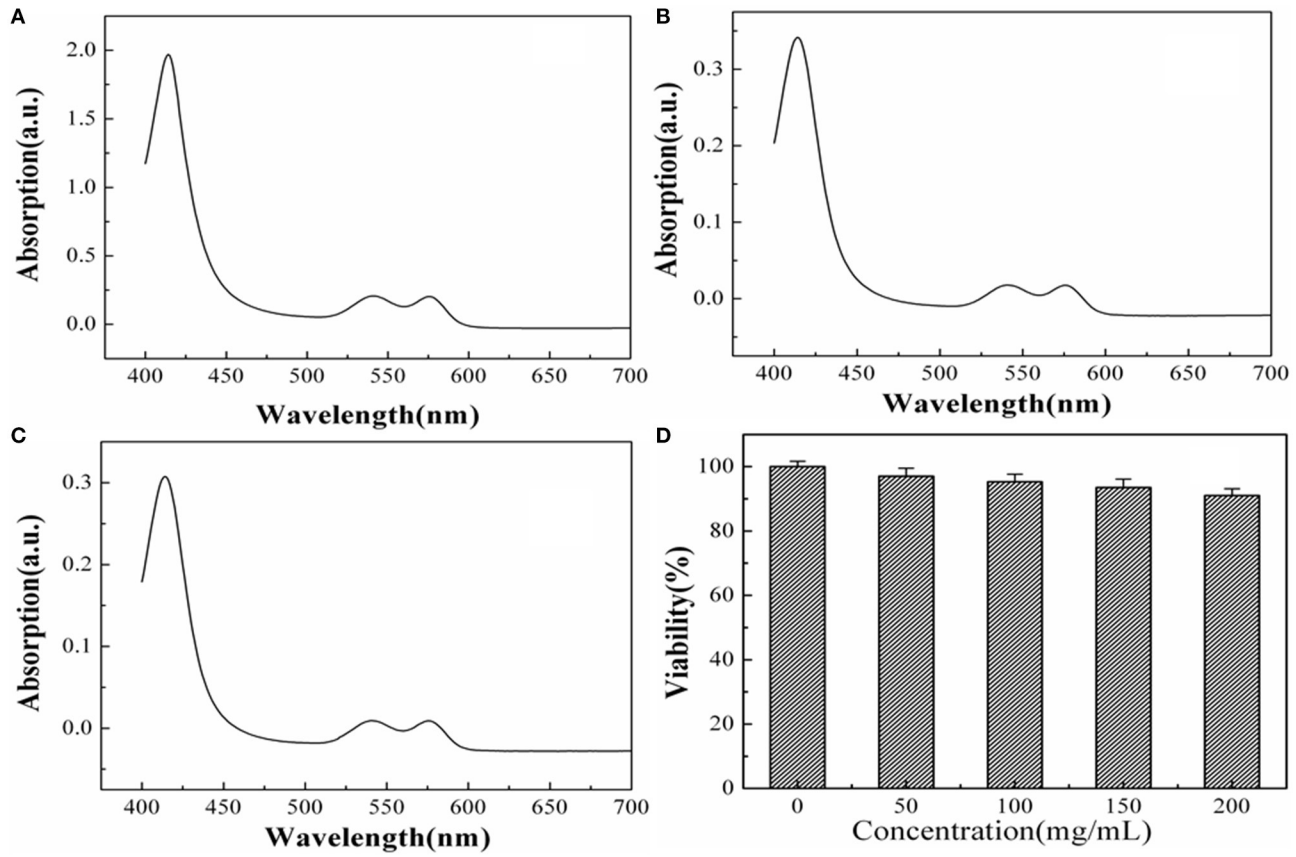

FIGURE 5 | The absorption curves of positive groups **(a)**, experimental groups **(b)**, and negative groups **(c)**. The cell viability of BaF_2:Nd NPs on HeLa cells at the concentration of 50–200 μg mL^{-1} with an incubation time of 48 h **(d)**.

The Images of BaF_2:Nd NP Dispersions in Phantom and Pork Tissues

To measure the luminescence signal of BaF_2:Nd NPs in biological tissues, a standard polyethylene phantom with similar optical parameter to mice muscle was used as a model; the capillary tube with a diameter of 0.2 mm was filled with NP dispersions and inserted into the hole of the phantom, under the excitation wavelength of 808-nm laser (80 mW cm^{-2}), and images with a penetration depth of 10 mm were acquired.

To test the spatial resolution of BaF_2:Nd NPs, two capillary tubes filled with NP dispersions (4 mg/mL) were inserted into two holes of the phantom (**Figure 7a**). Under the irradiation of 808-nm laser (80 mW cm^{-2}), images with a penetration depth of 7 mm were acquired. It can be seen that the two capillaries can be clearly distinguished with an interval of 2 cm inside the phantom (**Figure 7b**). By the same method, two capillary tubes with a diameter of 0.3 mm were inserted into the pork tissue, and images in the pork were recorded with a penetration depth of 5 mm (**Figure 7c**), which is higher than the imaging depth of GdF_3:Nd and LaF_3:Nd NPs (4 mm) [24, 25]. The luminescence intensity dropped to 65% of the original value in phantom due to the light attenuation resulting from the high absorption and scattering of biological tissue and water. When the excitation light penetrates the tissues, they become heavily decayed due to the absorption of water and fat. Therefore, the effective energy for excitation is reduced correspondingly. On the other hand, the attenuation of emission light is also inevitable when it penetrates all the biological tissues and the skin to be detected. A high spatial resolution of 300 μm was visualized, and the fluorescence images with a high signal-to-background ratio of

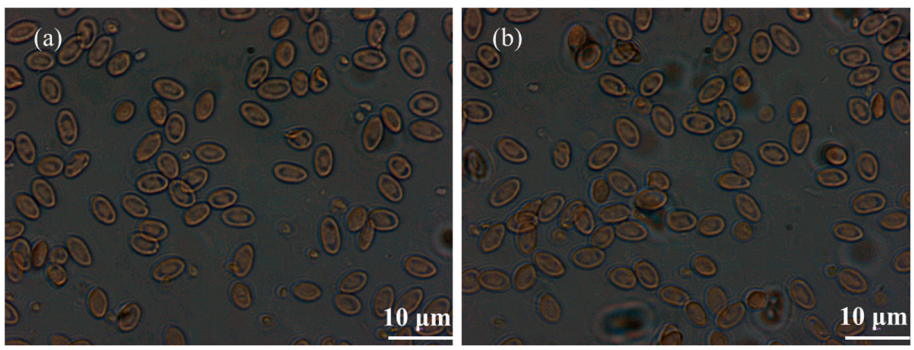

FIGURE 6 | The morphologies of RBCs captured by optical microscope: **(a)** the control group and **(b)** the BaF_2:Nd NP dispersion group.

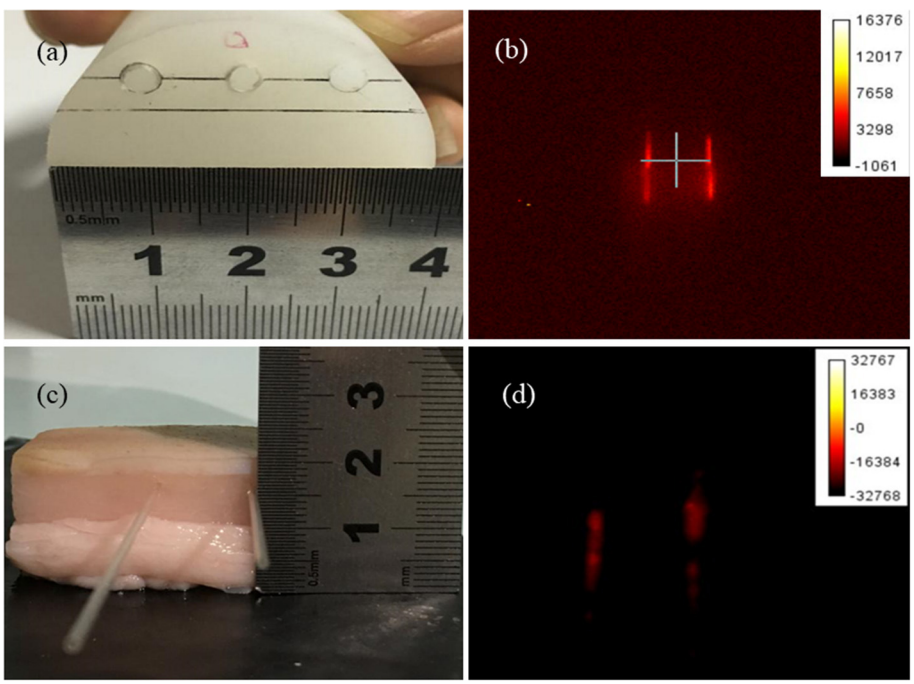

FIGURE 7 | The photographs of the phantom **(a)** and pork tissues **(c)**, and the NIR images of BaF_2:Nd NP dispersion (4 mg/mL) in the phantom **(b)** and pork tissues **(d)**.

18:1 were recorded in the pork tissue (**Figure 7d**). These high-quality images demonstrated the potential for advancement of this type of NP for deep tissue imaging in a living body.

CONCLUSION

A high fluorescence BaF_2:Nd NP without ligand was fabricated with a simple hydrothermal method. The NP dispersions exhibit high superior photostability and physical stability. Furthermore, an imaging depth of 5 mm and a high spatial resolution of 300 μm were found in the pork tissues. The fluorescence image shows a significant SBR of 18:1. Moreover, the BaF_2:Nd NPs show low HR value (3.27%) and high cell viability (91%). These superior performances of these nanoprobes exhibit their great potential application in high-contrast imaging and practical tumor diagnosis.

DATA AVAILABILITY STATEMENT

The raw data supporting the conclusions of this article will be made available by the authors, without undue reservation.

ETHICS STATEMENT

The studies involving human participants were reviewed and approved by the Ethics Committee of First Affiliated Hospital of Xi'an Jiaotong University. The patients/participants provided written informed consent to participate in this study.

AUTHOR CONTRIBUTIONS

XXC and HTG designed experiments. YTX and SFS carried out experiments. XSX and CQH analyzed experimental results. All authors contributed to the article and approved the submitted version.

FUNDING

This work was financially supported by the National Natural Science Foundation of China (Grant Nos. 61205039 and 61475189) and Natural Science Basic Research Plan in Shaanxi Province of China (Grant No. 2014JQ8345).

REFERENCES

1. Lei X, Li R, Tu D, Shang X, Liu Y, You W, et al. Intense near-infrared-II luminescence from $NaCeF_4$: Er/Yb nanoprobes for *in vitro* bioassay and *in vivo* bioimaging. *Chem Sci.* (2018) 9:4682–8. doi: 10.1039/C8SC00927A
2. Weissleder R. A clearer vision for *in vivo* imaging. *Nat Biotechnol.* (2001) 19:316–7. doi: 10.1038/86684
3. Wang X, Shi J, Li P, Zheng SH, Sun X, Zhang HW. $LuPO_4$: Nd^{3+} nanophosphors for dual-mode deep tissue NIR-II luminescence/CT imaging. *J Lumin.* (2019) 209:420–6. doi: 10.1016/j.jlumin.2019.02.028
4. Yang Q, Li X, Xue Z, Li Y, Jiang MY, Zeng S. Short-Wave near-infrared emissive $GdPO_4$:Nd^{3+} theranostic probe for *in vivo* bioimaging beyond 1300 nm. *RSC Adv.* (2018) 8:12832–40. doi: 10.1039/C7RA12864A
5. Fan Y, Wang PY, Lu YQ, Wang R, Zhou L, Zheng X, et al. Lifetime-engineered NIR-II nanoparticles unlock multiplexed *in vivo* imaging. *Nat Nanotech.* (2018) 13:941–6. doi: 10.1038/s41565-018-0221-0
6. Guo B, Feng Z, Hu DH, Xu SD, Middha E, Pan YT, et al. Precise deciphering of brain vasculatures and microscopic tumors with dual NIR-II fluorescence and photoacoustic imaging. *Adv Mater.* (2019) 31:1902504. doi: 10.1002/adma.201902504
7. Feng ZJ, Yang YM, Zhang J, Wang K, Li YX, Xu H, et al. *In vivo* and *in situ* real-time fluorescence imaging of peripheral nerves in the NIR-II window. *Nano Res.* (2019) 12:3059–68. doi: 10.1007/s12274-019-2552-z
8. Cao J, Zhu H, Deng D, Xue B, Tang L, Mahounga D, et al. *In vivo* NIR imaging with PbS quantum dots entrapped in biodegradable micelles. *J Biomed Mater Res Part A.* (2012) 100A:958–68. doi: 10.1002/jbm.a.34043
9. Chinnathambi S, Shirahata N. Recent advances on fluorescent biomarkers of near-infrared quantum dots for *in vitro* and *in vivo* imaging. *Sci Tech Adv Mater.* (2019) 20:337–55. doi: 10.1080/14686996.2019.1590731
10. Ren Y, He SQ, Huttad L, Chua MS, So SK, Guo QY, et al. NIR-II/MR dual modal nanoprobe for liver cancer imaging. *Nanoscale.* (2020) 12:11510–7. doi: 10.1039/D0NR00075B
11. Pan Z, Wen Y, Wang T, Wang K, Teng YJ, Shao K. One-step synthesis of hollow PEI-$NaBiF_4$: Yb^{3+} /Er^{3+} upconversion nanoparticles for water-responsive luminescent probe. *J Rare Earth.* (2019) 38:362–8. doi: 10.1016/j.jre.2019.04.022
12. Liu S, Li W, Gai S, Yang GX, Zhong CN. A smart tumor microenvironment responsive nanoplatform based on upconversion nanoparticles for efficient multimodal imaging guided therapy. *Biomater Sci.* (2019) 7:951–62. doi: 10.1039/C8BM01243A
13. Cho SK, Su LJ, Mao C, Wolenski CD, Flagi TW, Park W. Multifunctional nano-clusters of $NaYF_4$:Yb^{3+}, Er^{3+} upconversion nanoparticle and gold nanorod for simultaneous imaging and targeted chemotherapy of bladder cancer. *Mater Sci Eng C Mater Biol Appl.* (2019) 97:784–92. doi: 10.1016/j.msec.2018.12.113
14. Ma L, Huang S, He SQ, Wang ZX, Cheng Z. Polydopamine-coated downconversion nanoparticle as an efficient dual-modal near-infrared-II fluorescence and photoacoustic contrast agent for non-invasive visualization of gastrointestinal tract *in vivo*. *Biosens Bioelectron.* (2020) 151:112000. doi: 10.1016/j.bios.2019.112000
15. Tan M, Del RB, Zhang Y, Martín RE, Hu J, Zhou ZG, et al. Rare-earth-doped fluoride nanoparticles with engineered long luminescence lifetime for time-gated *in vivo* optical imaging in the second biological window. *Nanoscale.* (2018) 10:17771–80. doi: 10.1039/C8NR02382D
16. Zhang WJ, Yu DC, Zhang JP. Near-infrared quantum splitting in Ho 3+:LaF 3 nanocrystals embedded germanate glass ceramic. *Opt Mater Exp.* (2012) 2:636–43. doi: 10.1364/OME.2.000636
17. Yu DC, Ye S, Huang XY. Enhanced three-photon near-infrared quantum splitting in β-$NaYF_4$:Ho^{3+} by codoping Yb $^{3+}$. *AIP Adv.* (2012) 2:022124. doi: 10.1063/1.4718412
18. Zhao Z, Yuan J, Zhao X, Bandla A, Thakor NV, Tan MC. Engineering the infrared luminescence and photothermal properties of double-shelled rare-earth-doped nanoparticles for biomedical applications. *ACS Biomater Sci Eng.* (2019) 5:4089–101. doi: 10.1021/acsbiomaterials.9b00526
19. Liu G, Sun Z, Jia M, Fu ZL, Zhang AQ, Li PP. One pot synthesis and optimized luminescent intensity of Gd_2 $(WO_4)_3$:Yb^{3+}/Ho^{3+}@SiO_2 nanoparticles for biological application. *J Lumin.* (2019) 206:1–5. doi: 10.1016/j.jlumin.2018.10.039
20. Cui X, Fan Q, Shi S. A novel near-infrared nanomaterial with high quantum efficiency and its applications in real time *in-vivo* imaging. *Nanotech.* (2018) 20:205705. doi: 10.1088/1361-6528/aab2fa
21. Andrade AB, Ferreiraab NS, Valerio MEG. Particle size effects on structural and optical properties of BaF_2 nanoparticles. *RSC Adv.* (2017) 7:26839–48. doi: 10.1039/C7RA01582H
22. Ding Y, Du C, Qian JW, Dong CM. Zwitterionic polypeptide nanomedicine with dual NIR/reduction-responsivity for synergistic cancer photothermal-chemotherapy. *Polym Chem.* (2019) 10:4825–36. doi: 10.1039/C9PY00986H
23. Duan W, Zhang Y, Wang Z. Synthesis and near-infrared fluorescence of $K_5NdLi_2F_{10}$ nanocrystals and their dispersion with high doping

concentration and long lifetime. *Nanoscale.* (2014) 6:5634–8. doi: 10.1039/c3nr06825k

24. Mimun LC, Ajithkumar G, Pokhrel M, Yust BG, Elliott ZG, Pedraza F, et al. Bimodal imaging using neodymium doped gadolinium fluoride nanocrystals with near-infrared to near-infrared downconversion luminescence and magnetic resonance properties. *J Mater Chem B.* (2013) 1:5702–10. doi: 10.1039/c3tb20905a
25. Rocha U, Kumar KU, Jacinto C, Villa I, Sanz-Rodríguez F, Iglesias de la Cruz Mdel C, et al. Neodymium-Doped LaF_3 Nanoparticles for fluorescence bioimaging in the second biological window. *Small.* (2014) 10:1141–54. doi: 10.1002/smll.201301716

Conflict of Interest: The authors declare that the research was conducted in the absence of any commercial or financial relationships that could be construed as a potential conflict of interest.